Journal of Hydroscience and Hydraulic Engineering
Vol. 19, No.1 May, 2001, 141-152

NUMERICAL STUDY OF 2-D PARTICLE CLOUDS AND EFFECT OF TURBIDITY FENCES

Juichiro Akiyama, Akhilesh Kumar Jha, Xinya Ying and Masaru Ura

By

Department of Civil Engineering, Kyushu Institute of Technology
Tobata, Kitakyushu 804-8550, Japan.

SYNOPSIS

The motion of 2-D particle clouds with and without a turbidity fence is numerically investigated. A numerical model, utilizing the concept of the large-eddy simulation, is developed for the purpose. The governing equations comprising of a filtered 2-D Navier-Stokes equations and the mass transport equation are solved through operator-splitting algorithm using implicit cubic spline interpolation in space and the Crank-Nicolson scheme in time. The eddy viscosity is evaluated by the Smagorinsky model, modified to include the buoyancy term. Numerical results for such main flow characteristics as shape, size, average buoyancy and moving speed of the particle cloud as well as the amount of particles deposited on the bed are compared with experimental data. The comparison shows that the numerical model can predict the motion of particle clouds in the whole process, from the falling to spreading stage. The effect of turbidity fence on the motion and containment of the particle cloud is also reasonably simulated by the model.

INTRODUCTION

Dredged materials, soil and rubble are often dumped into coastal waters during such works as construction of man-made islands, disposal of industrial wastes and reclaiming of coastal areas. Besides the intended outcome of these actions, the effect extends to changed floor topography and water quality in a large area adjoining the dumping site. The prediction of amount and extent of diffusion of turbidity resulting from dumping such materials is of practical importance for assessing the environmental impact on plankton, benthic organisms and fishes near the disposal site. The information obtained from such predictions can then be used to formulate ways and means to minimize the extent of any adverse effects.

The buoyant clouds, consisting of fine particles in particular, formed by instantaneous releases of such materials fall under the action of their own buoyancy. A buoyant cloud falling under its own buoyancy is said to be in the falling stage. Nakatsuji et al.(1) theoretically and experimentally studied the falling stage of particle clouds and found that particle clouds behave like their homogeneous counterparts if the initial volume is large and the particle size is relatively small. Buhler and Papantoniou(2) conducted a theoretical and experimental study on swarms of coarse particles. They found that in the final stage, the front velocity remains constant and somewhat larger than the mean settling velocity of particles.

Oda et al. (3) numerically investigated the settling and spreading behavior of particle clouds using the improved DEMAC method. Li (4) studied particle clouds experimentally and numerically, and concluded that the velocity of the clouds approaches the terminal settling velocity of the individual particles and the growth rate of half width of clouds decreases with the magnitude of the settling velocity of particles.

After impinging on the bottom, the falling stage ends and the cloud spreads along the bed. This may be referred to as the spreading stage. In contrast to the investigations of the falling stage, only few studies have been performed on this stage. Tamai et al.(5) extended the thermal theory to investigate the spreading stage of two-dimensional particle clouds formed by releasing a fixed volume of sand into waters with finite depth, and theoretically and experimentally found that the motion of particle clouds is dependent on the sand size. Tamai and Muraoka (6) qualitatively investigated turbidity transport produced by direct dumping of soil using the two-fluid model. They reported that the induced flow is depressed by slowing down the rate of dumping of soil.

In this study, the motion of buoyant clouds formed by releasing fine particles into quiescent water with finite depth is studied numerically. The spreading stage of the clouds is investigated with and without a

turbidity fence. A dispersion model was chosen to model the particle phase. The model simulates turbulence by the large-eddy simulation (LES). The validity of the numerical model is extensively tested against experimental data for the whole process of the motion of the particle clouds, from the falling to spreading stage. Comparisons of the main flow characteristics between the particle and the saline clouds are made as well. The effect of turbidity fence of different height placed at different locations is also investigated that yields important conclusions.

EXPERIMENTS

The motion of a two-dimensional particle cloud, formed by instantaneously releasing a fixed volume of water-particle mixture into quiescent waters with finite depth, is schematically illustrated in Fig.1, in which W_0 = half of total buoyancy force of the cloud in the falling stage ($=A_0 g(\rho_0 - \rho_a)/\rho_a$), A_0 = half volume of the cloud per unit width in the falling stage, ρ_0 = initial density of the cloud, ρ_a = density of ambient fluid, g = acceleration due to gravity, h = water depth, H, L, B and V = half width, length, average buoyancy and mass center velocity of the cloud in the falling stage, respectively, H_g, B_g and V_{fg} = height, average buoyancy and front propagation speed of the cloud in the spreading stage, respectively, W_d = buoyancy of deposited particles per unit length and W_s = total buoyancy of the cloud in the spreading stage.

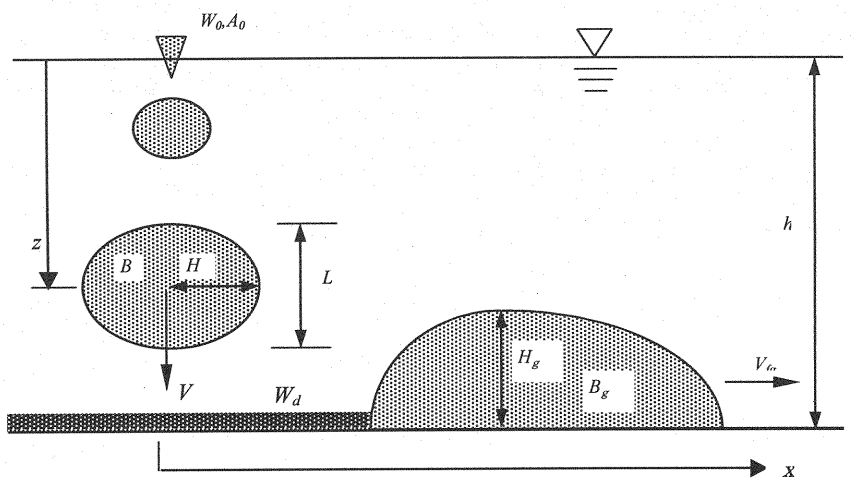

Fig. 1 Sketch of a particle cloud released into quiescent waters with finite depth

Table 1. Experimental conditions

Case	Matter to form cloud	Special gravity of particles, s_p	Mean diameter of particles, d_{50} (mm)	$\varepsilon_0=(\rho_0-\rho_a)/\rho_a$	W_0 (m^3/s^2)
P1	Glass bead	2.47	0.044	0.194	0.00475
P2	Glass bead	2.47	0.088	0.124	0.00303
P3	Sand	2.65	0.140	0.194	0.00475
P4	Glass bead	2.47	0.044	0.200	0.00490
S1	Saline	--	--	0.200	0.00490

Five sets of experiments were carried out in a glass flume of 7.5m length, 1.0m height and 0.1m width. The experimental conditions are given in Table 1. The water depth in the glass flume was kept constant at 0.9m in all cases. The particle clouds were formed by releasing glass beads for cases P1, P2 and P4, and sand for case P3. For case S1, the buoyant cloud was formed by releasing saline water. The whole process,

from the falling to the spreading stage is studied in cases P4 and S1. In other cases, the attention is focused on the falling stage only. In all cases, a fixed volume ($2A_0$=0.005m^2) of particle-water mixture or saline water was instantaneously released into waters by a device placed just above water surface.

The motion of the buoyant clouds was recorded by a VTR-camera moving with the clouds. The speed and the geometry of the clouds were obtained from the analysis of the recorded images. To minimize experimental errors, an experiment was repeated five times under the same conditions. The experimental results on the geometry and speed of the clouds presented herein are average values of such five measurements. Average buoyancy of the falling stage, B was calculated by assuming the conservation of total buoyancy. Average buoyancy in the spreading stage B_g for the saline cloud was estimated from the density distribution measured by conductivity meter and for the particle clouds from the mass of particles contained in the clouds, which was measured by separating a particle cloud using two slide gates and subsequently collecting the separated particles with a siphon tube. To obtain the profiles of B_g along distance, the measurements were carried out at five different sections along the flume, repeating measurements at each section three times under the same experimental conditions. The buoyancy of deposited particles per unit length, W_d was determined by collecting the particles deposited on the bed by a siphon after deposition of the suspended particles was complete. The experimental data for B_g, and W_d used in this paper are the average of three measurements for these under the same experimental conditions.

MODEL FORMULATION

A dispersion model is used to numerically model the particle phase. In the model, the particle phase is treated as a continuous fluid and the slip velocity between fluid phase and particle phase is assumed to be the settling velocity of particles. This model, efficient when particles are relatively finer and the cloud is relatively denser, has been successfully used previously, as in the numerical studies of convection of particle thermals by Li (4) and for sediment transport in open channel by Celik and Rodi (7).

Applying the grid-filter to the incompressible Navier-Stokes equations and mass transport equation, the governing equations for the mean-flow and mass transport are obtained as

$$\frac{\partial U_i}{\partial x_i} = 0 \tag{1}$$

$$\frac{\partial U_i}{\partial t} + U_j \frac{\partial U_i}{\partial x_j} = -\frac{1}{\rho_a}\frac{\partial P}{\partial x_i} + \nu \frac{\partial^2 U_i}{\partial x_j^2} + \frac{\partial}{\partial x_j}\left(-\overline{u_i' u_j'}\right) + g_i \frac{\Delta\rho}{\rho_a} \tag{2}$$

$$\frac{\partial C}{\partial t} + (U_i + V_{si})\frac{\partial C}{\partial x_i} = \frac{\partial}{\partial x_i}\left(-\overline{u_i' c'}\right) \tag{3}$$

where U_i= velocity component in the direction x_i; P = pressure minus the hydrostatic pressure at reference density ρ_a; ρ = density; $\Delta\rho$ = density excess (= ρ - ρ_a); g_i = component of acceleration due to gravity in the direction x_i; u_i' = fluctuating velocity; C= volume concentration of particles or dense fluid; c' = fluctuating concentration; $\overline{u_i' c'}$ = subgrid correlation terms between fluctuating velocity and concentration; V_{si} = settling velocity of particles in the direction x_i; and $\overline{u_i' u_j'}$ = subgrid correlation terms between fluctuating velocity due to the grid-filtering, expressed as

$$-\overline{u_i' u_j'} = \nu_t\left(\frac{\partial U_i}{\partial x_j} + \frac{\partial U_j}{\partial x_i}\right) - \frac{2}{3}k\delta_{ij} \tag{4}$$

where k = turbulent kinetic energy; δ_{ij} = Kronecker delta function; ν_t = subgrid scale eddy viscosity which, under the assumption that the subgrid turbulent production includes a buoyancy term (8), can be expressed as;

$$\nu_t = (Cs\Delta)^2\left(|\bar{S}|^2 - \frac{g_i}{\rho Sc_t}\frac{\partial \Delta\rho}{\partial x_i}\right)^{1/2} \tag{5}$$

where Δ = filter width; Cs = Smagorinsky constant; and $|\bar{S}| = (2\bar{S}_{ij}\bar{S}_{ij})^{1/2}$ = magnitude of large-scale strain rate tensor in which $\bar{S}_{ij}$ is given by

$$\bar{S}_{ij} = \frac{1}{2}\left(\frac{\partial U_i}{\partial x_j} + \frac{\partial U_j}{\partial x_i}\right) \tag{6}$$

The term $-\overline{u_i'c'}$ in Eq. (3) is generally assumed to be expressed as

$$-\overline{u_i'c'} = \frac{\nu_t}{Sc_t}\frac{\partial C}{\partial x_i} \tag{7}$$

where Sc_t = subgrid turbulent Schmidt number.

The last term in Eq. (4) represents the normal stresses and can be absorbed in the pressure terms of the momentum equations. Eqs. (1), (2) and (3) are solved by the operator-splitting algorithm and the Crank-Nicolson method-based cubic spline interpolation (CCS) scheme, the details of which are referred to Ying et al. (9).

COMPUTATIONAL CONDITIONS

For cases P1, P2 and P3, the computational domain is a rectangle of 2.0m width and 1.4m height. All boundaries are considered as slip wall boundaries. The initial buoyant clouds have the same values of A_0 and W_0 as those in the experiments, centered at the centerline of the domain and 3 times of initial half width below water surface.

For cases S1 and P4, computational domain is a rectangle of 10.0m width and 0.9m height. The imposed boundary conditions for velocity, pressure and concentration are

$$V_\tau = 0, \quad V_n = 0 \qquad \text{(bottom boundary)}$$

$$\frac{\partial V_\tau}{\partial n} = 0, \quad \frac{\partial V_n}{\partial n} = 0 \qquad \text{(side boundaries)}$$

$$\frac{\partial V_\tau}{\partial n} = 0, \quad V_n = 0 \qquad \text{(top boundary)}$$

$$\frac{\partial P}{\partial n} = 0, \quad \frac{\partial C}{\partial n} = 0 \qquad \text{(all boundary)}$$

In the spreading stage, an additional boundary condition is needed for the equation of mass conservation to take into account deposition of particles. In a sediment-laden open channel flow, the net-deposition rate D is commonly assumed to be proportional to free settling velocity V_s and near-bed reference concentration C_b. However, for general situations there is no accurate way to determine the net-deposition rate to the bed. In this study, we assume that D has an expression similar to that for a sediment-laden open channel flow, that is

$$D = \alpha V_s C_b \tag{8}$$

where α = empirical coefficient.

Numerical simulations with different trial values of α yields a value of $\alpha = 2$ for which deposition of particles in numerical computations agrees with that in the experiments (Fig.9). A probable reason for the value of $\alpha > 1$ is that the effective settling velocity of particles in the presence of turbulence is larger than the settling velocity of individual particle V_s.

Grid size in all cases was 0.01m×0.01m. Time step was 0.01s. The value of Cs was determined as 0.16 for both saline and particle clouds. The value of Sc_t for saline cloud was taken as 0.1 while that for particle cloud was obtained as 0.2. These values of Cs and Sc_t have been obtained by comparing computational results with experimental results for the falling stage. It is not surprising that there is a

difference in the value of Sc_t between the saline and the particle clouds, because Sc_t depends on the local turbulence intensity and the molecular value Sc that varies with diffusing material (10). For the spreading stage, the values of C_s and Sc_t are kept the same as that obtained for the falling stage.

Note that for convenience, the free water surface is treated as a horizontal rigid boundary in the computation. A comparison of computational and experimental results in the following would support this assumption as a reasonable simplification.

NUMERICAL RESULTS

Qualitative analyses:

Photographs, computed concentration and velocity fields of the particle cloud for case P4 are shown in Fig.2. The figures at t = 4 s show the particle cloud in the falling stage. The figures at t = 49 s show the particle cloud in the spreading stage following the impingement of the particle cloud on the bottom soon after

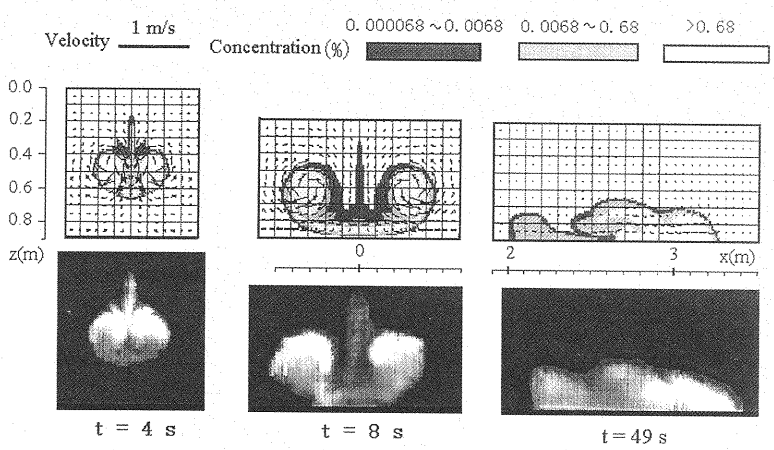

Fig.2 Photographs and computed velocity and density excess fields for case P4

t = 8 s. It can be seen from these figures that shape, size and speed of the cloud are well simulated by the model. It is also observed that the particle cloud, like a saline cloud (9), also has a wake and a flow-structure of two symmetrical vortexes. Due to the entrainment of less dense ambient fluid into the central part from the rear of the cloud, a reverse mushroom shaped cloud is gradually formed (t = 8 s). After impingement, the cloud splits into two parts and each one propagates in the opposite direction along the horizontal bottom (t = 49 s). The flow becomes weaker with the distance, finally vanishing due to the settling of particles.

Quantitative analyses for falling stage:

In Figs.3-5, the computed results for non-dimensional half width H^*, average buoyancy B^* and mass center velocity V^* of particle clouds are presented, along with those for the saline cloud, in which the non-dimensional quantities are defined as $x_f^* = x_f / A_0^{1/2}$, $H_g^* = H_g / A_0^{1/2}$, $B_g^* = B_g/(W_0/A_0)$, $V_{fg}^* = V_{fg}/(W_0^2 / A_0)^{1/4}$, x_f=horizontal distance measured from the center of initial buoyant clouds to the front of horizontally spreading clouds. It is observed that the motion of the cloud composed of finer particles, as in case P1, is well simulated and its H^*, B^* and V^* are close to that of the saline cloud. For case P2, in which the settling velocity of particles V_s is about 4 times larger than that in case P1, the reasonable agreements between the computational and the experimental results are achieved. For case P3, in which the settling velocity of particles V_s is about 10 times larger than that in case P1, the computed H^*, B^* and V^* significantly differ from the experimental results. These comparisons seem to indicate that the present model works better if the settling velocity of particles remains less than 1/10 of the mass center velocity of the clouds.

Quantitative analyses for spreading stage:

Figs.6-8, compare computed and observed results for non-dimensional height H_g^*, average buoyancy B_g^* and front propagation speed V_{fg}^* of the particle cloud and the saline cloud with the same W_0. It can be

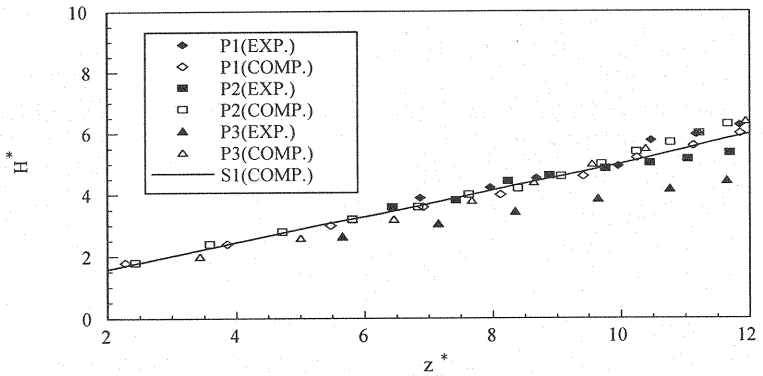

Fig.3 H^* as a function of z^*

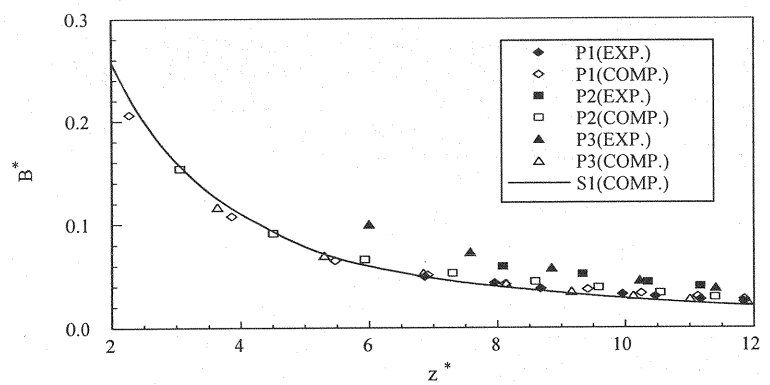

Fig.4 B^* as a function of z^*

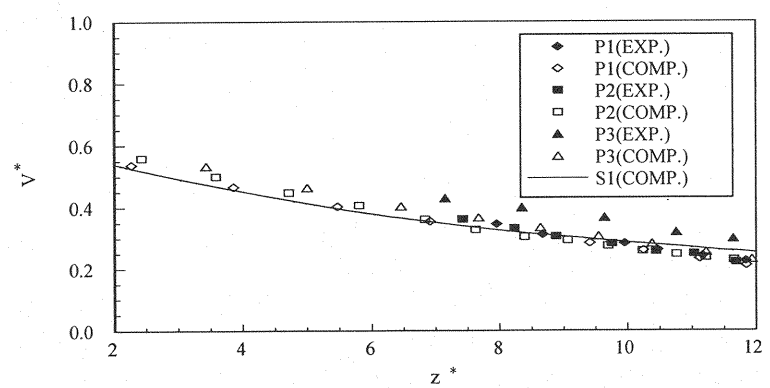

Fig.5 V^* as a function of z^*

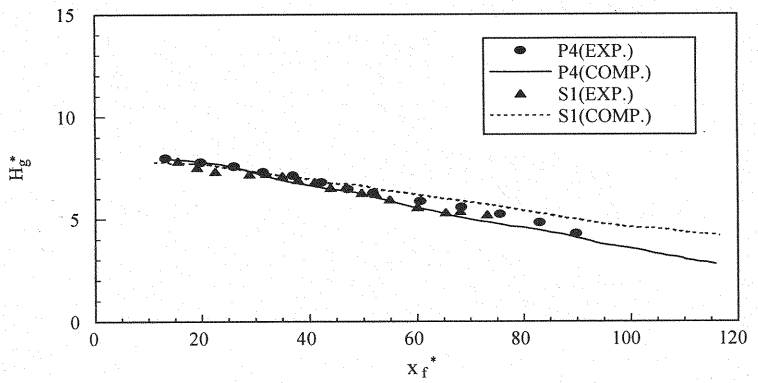

Fig.6 H_g^* as a function of x_f^*

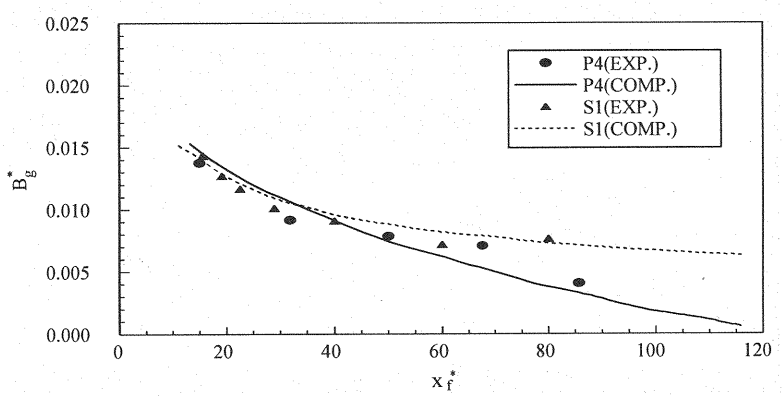

Fig.7 B_g^* as a function of x_f^*

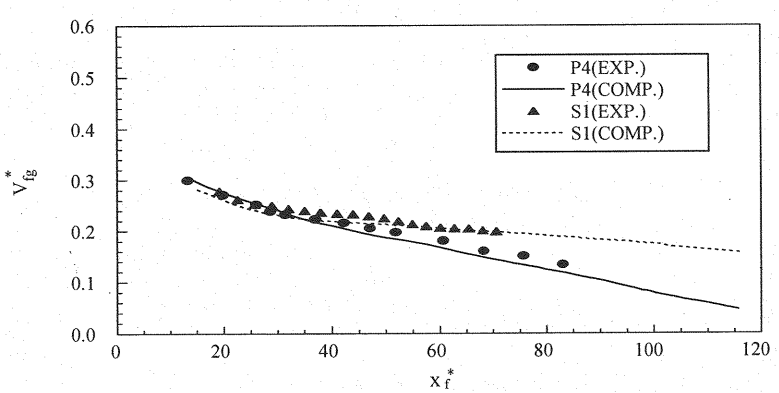

Fig.8 V_{fg}^* as a function of x_f^*

seen that H_g^*, B_g^* and V_{fg}^* are very well predicted. The decrease in these flow characteristics along distance for the particle cloud is more rapid than the saline cloud because of settling of particles to the bed.

The buoyancy of deposited particles per unit length as a function of distance is presented in Fig.9, in which $W_d^* = W_d / W_0$. Both experimental and computed results show that the amount of the deposit increases

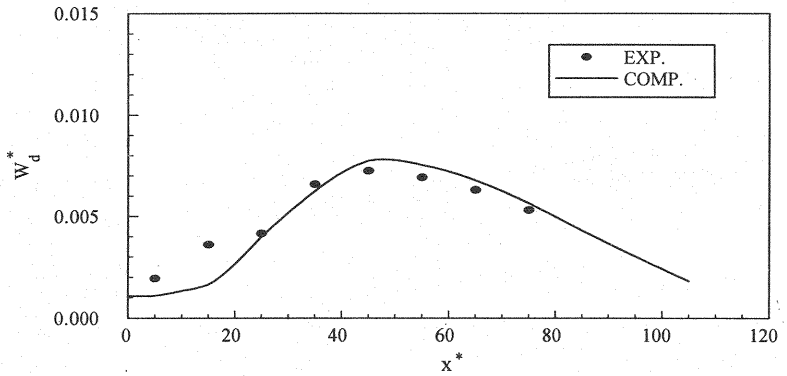

Fig.9 W_d^* as a function of x^* for case P4

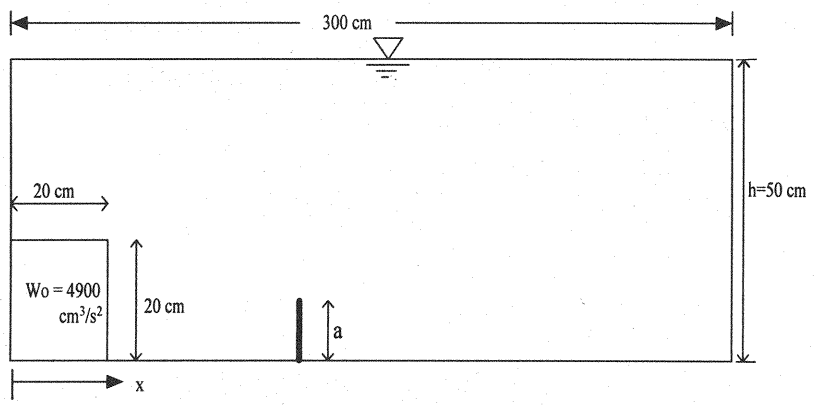

Fig.10 Computational domain for investigating effects of turbidity fence

from a relatively small value at the impingement point to a maximum value at about x^*=46 and then decreases towards zero. This deposit profile is formed because in the earlier times after the impingement, the circulating motion is relatively strong and most of the particles are in suspension, as shown in Fig.2 (t=8s). As the cloud moves forward, the motion becomes weaker, as shown in Fig.2 (t=49s), so that the deposition of particles increases.

EFFECTS OF TURBIDITY FENCE

Turbidity fences are used as an effective tool for partial or total containment of the spreading of particles. The present model can be used to determine the location and height of a turbidity fence needed for the intended level of containment. The capability of the model for such computations is shown by investigating spreading of a particle cloud following sudden release of particle-water mixture through a gate opening. The computational domain is shown in Fig.10. The reservoir is 3 m long and contains 0.5m deep still water. The initial total buoyancy, W_s of the particle-water mixture, within a 0.2m x 0.2m area, is 0.0049 m^3/s^2. A gate separates this mixture from the ambient water. The gate is released at the start of computation and the computation is continued till the changes in buoyancy in all cells become insignificant.

The computations are carried out with varying location and height of the 0.04m thick turbidity fence. Five computations are carried out at each location with the height of the turbidity fence, a = 0.0, .05, 0.1, 0.15 and 0.2m. The typical motion of a particle cloud passing over a 0.05m high turbidity fence placed at x=1.0m is shown in Fig.11. It is observed that while the lower layers of high concentrations are effectively blocked the fence, part of the cloud spills over to the other side of the fence.

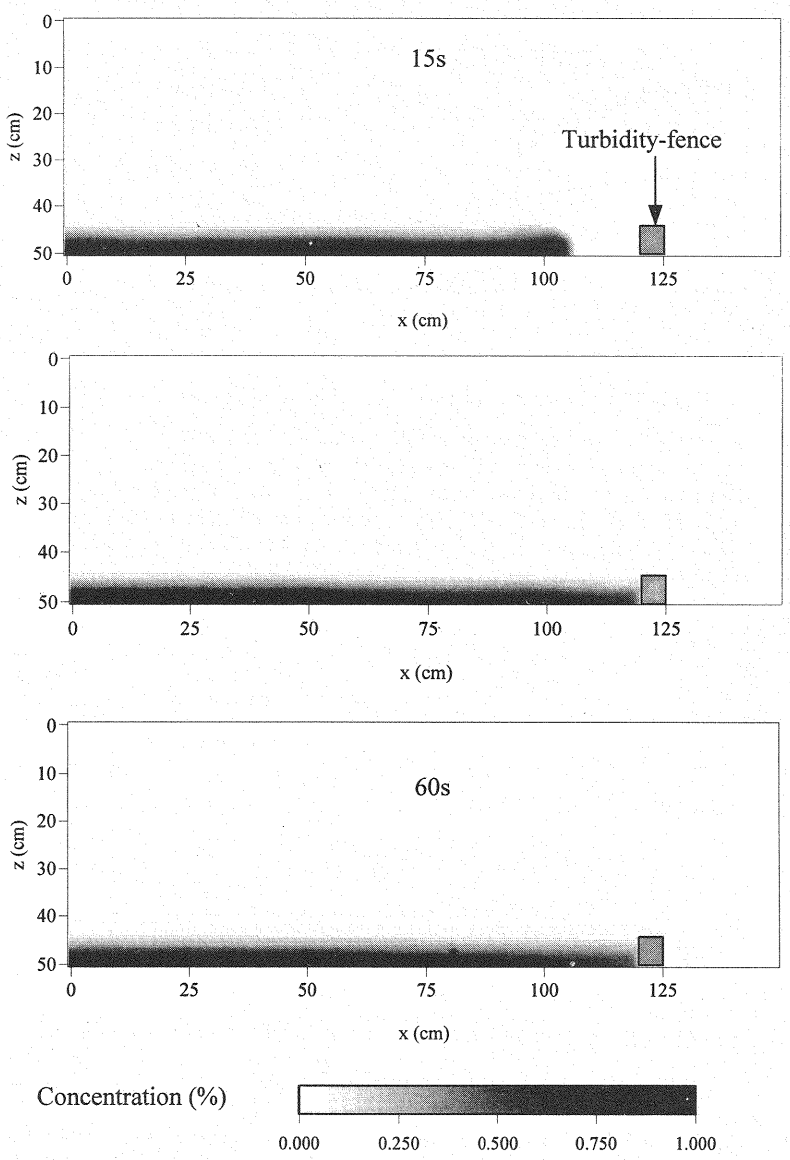

Fig.11 Motion of a particle cloud passing over a turbidity fence

Fig.12 shows the containment of the particle cloud by the fence. The line without symbols shows the final deposition of particles along the reservoir without any fence. The presence of the fence blocks most of the particles allowing only a small amount to cross over. The particles crossing over the fence also settle down close to the fence due perhaps to the retardation effect of the turbidity fence.

Fig.13 shows the non-dimensional plot of buoyancy of the particles passing over fence $W_{d\,t}$ ($=\Sigma\, W_d^*$) for different height placed at three distances from the gate. It is observed that at a given location, the amount of particles passing that location drops drastically even for a lower fence height. Thereafter, the incremental benefit for increased height of the fence gradually reduces. That is so because the lower layers of the moving cloud have higher concentration and once these layers are contained then any increment in the fence height works only on the upper portions of the cloud which are low in concentration. As may be expected, the height of the fence needed for same level of containment is more when the fence is placed nearer to the gate.

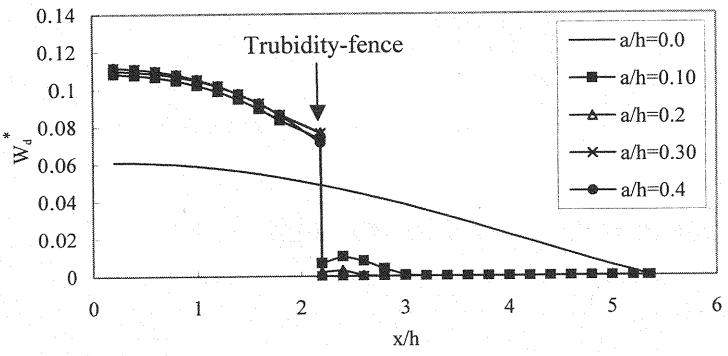

Fig.12 Containment of particle cloud by turbidity fence

As the fence height is increased to 0.2 m the cloud is fully contained behind the fence. It appears that this height may be related to the maximum height of the cloud on release from the gate. It is anticipated that unless the fence is placed extraordinarily close to the point of release, a fence height equal to the initial maximum height of the cloud might be sufficient. This example clearly demonstrates the effectiveness of turbidity fence in containing particle clouds as well as the present model's ability to compute propagation of particle clouds in the presence of turbidity fence.

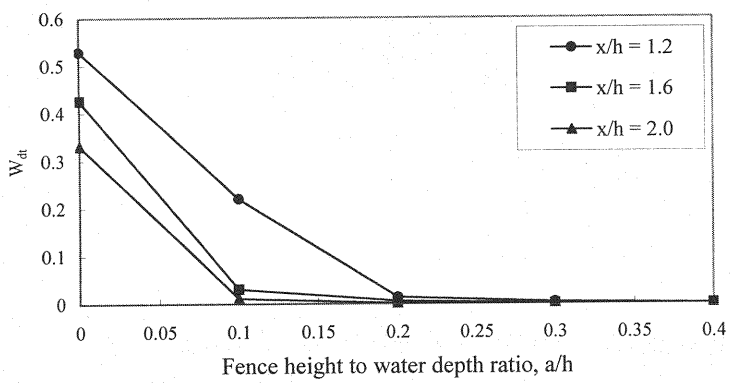

Fig.13 Particles passing over the fences of different height at different distances.

CONCLUSIONS

It may be concluded for the falling stage that if the settling velocity of particles V_{si} remains less than 1/10 of the mass center velocity V of the particle clouds, the numerical model with C_s=0.16 and Sc_t=0.2 can well predict the motion of the particle clouds. In addition, for the clouds composed of finer particles, variations of the non-dimensional half width H^*, the average buoyancy B^* and the mass center velocity V^* with the non-dimensional distance z^* are close to those of the saline cloud.

The numerical model can very well predict the non-dimensional height H_g^*, average buoyancy B_g^*, front propagation speed V_{fg}^* and buoyancy of deposited particles W_d^* in the spreading stage, using the same values of C_s and Sc_t as those in the falling stage. It is found that the non-dimensional height H_g^*, average buoyancy B_g^*, front propagation speed V_{fg}^* of the particle cloud decrease more rapidly with non-dimensional distance x^* than those of the saline counterpart, because of settling of particles.

The numerical model can well simulate the complex motion of the particle clouds passing over the

turbidity fence. The model can be used to determine height and position of a turbidity fence needed for desired level of containment.

ACKNOWLEDGMENT

This study was supported by the Grant-in-Aid for Science Research of the Ministry of Education and Culture, Japan under the Grant B(2)12555149.

REFERENCE

1. Nakatsuji, K., Tamai, M. and Murota, A.: Dynamic behaviors of sand clouds in water, Int. Conf. Phys. Modelling of Transport and Dispersion, M.I.T. Boston, 8C.1-8C.6. 1990.
2. Buhler, J. and Papantoniou, D.A.: Swarms of coarse particles falling through a fluid, Proc. of Int. Symposium on Environmental Hydraulics, Vol.1, pp.135-140, 1991.
3. Oda, K., Shigematsu, T. Onishi, N. and Inoue, M.: Numerical simulation of settling and spreading behavior of particle cloud using improved DEMAC method, Proceedings of Coastal Engineering, JSCE, Vol.39, pp.971-975, 1992 (in Japanese).
4. Li, C.W.: Convection of particle thermals, Journal of Hydraulic Research, IAHR, Vol.35, No.3, pp.363-376, 1997.
5. Tamai, M., Muraoka, K., Murota, A. and Machida, H.: Study on initial stage of diffusion process of turbidity in direct dumping of soil, Journal of Hydraulic, Coastal and Environmental Engineering, JSCE, No.515/II-31, pp.77-86, 1995 (in Japanese).
6. Tamai, M. and Muraoka, K.: Numerical simulation on characteristics of turbidity transport generated in direct dumping of soil, Annual Journal of Hydraulic Engineering, JSCE, Vol.42, pp.541-546, 1998 (in Japanese).
7. Celik, I. and Rodi, W.: Modeling suspended sediment transport in nonequilibrium situations, Journal of Hydraulic Engineering, ASCE, Vol.114, No.10, pp1157-1191,1988
8. Eidson, T. M.: Numerical simulation of the turbulent Rayleigh-Benard problem using subgrid modeling, Journal of Fluid Mech., Vol.158, pp.245-268, 1985.
9. Ying, X., Akiyama, J. and Ura, M.: Motion of dense fluid released into quiescent water with finite depth, Journal of Hydraulic, Coastal and Environmental Engineering, JSCE, No.635/II-49, pp.141-152, Nov. 1999
10. Reynolds, A.J.: The prediction of turbulent Prandtl and Schmidt numbers, Int. J. Heat Mass Transfer, Vol.18, pp.1055-1069, 1975.

APPENDIX - NOTATION

The following symbols are used in this paper :

A_0 = half volume of the cloud per unit width in the falling stage;
a = height of turbidity fence;
B = buoyancy of the cloud in the falling stage;
B_g = average buoyancy of the cloud in the spreading stage;
C = volume concentration of particles or dense fluid;
C_b = near-bed reference concentration;
Cs = Smagorinsky constant;
c′ = fluctuating concentration;
d_{50} = mean diameter of particles;
g_i = specific body force in the direction x_i ;
H = half width of the cloud in the falling stage;
H_g = height of the cloud in the spreading stage;
h = depth of ambient water;
k = turbulent kinetic energy ;
L = length of the cloud in the falling stage;
P = pressure minus the hydrostatic pressure at reference density ρ_a ;
Sc_t = subgrid turbulent Schmidt number;

$|\overline{S}|$ = magnitude of large-scale strain rate tensor;
s_p = specific gravity of particles;
U_i = velocity component in the direction x_i;
u_i' = fluctuating velocity;
$\overline{u_i'c'}$ = subgrid correlation terms between fluctuating velocity and concentration;
$\overline{u_i'u_j'}$ = subgrid correlation terms between fluctuating velocity due to the grid-filtering;
V = mass center velocity of the cloud in the falling stage;
V_{fg} = front propagation speed of the cloud in the spreading stage;
V_n = velocity normal to the computational boundary;
V_{si} = settling velocity of particles in the direction x_i;
V_τ = velocity tangential to the computational boundary;
W_0 = half of total buoyancy force in the falling stage;
W_d = buoyancy of deposited particles per unit length;
W_s = total buoyancy of a particle cloud in the spreading stage;
x_f = front location;
$*$ = superscript denoting non-dimensionalized variables;
Δ = filter width;
$\Delta\rho$ = density excess ($=\rho - \rho_a$);
α = empirical coefficient for settling velocity;
$\delta_{i,j}$ = Kronecker delta function;
ε_0 = initial relative density difference;
ν_t = subgrid scale eddy viscosity;
ρ = density;
ρ_0 = initial density of the cloud; and
ρ_a = density of ambient fluid.

(Received August 25, 2000 ; revised December 22, 2000)